Supporting Information for " Numerical Analysis of the Effect of Heterogeneity on CO_2 Dissolution Enhanced by Gravity Driven Convection"

Yufei Wang[1,2] Daniel Fernàndez-Garcia[1,2] Maarten W. Saaltink[1,2]

[1]Dept. of Civil and Environmental Engineering, Universitat Politècnica de Catalunya, Jordi Girona 1-3, 08034 Barcelona, Spain

[2]Associated Unit: Hydrogeology Group (UPC-CSIC)

Contents of this file

Introduction

This supporting information is comprised of two sections. The first section (S1) shows how to choose the grid size for numerical simulation, and the second section (S2) gives detailed results on gravity driven convection in homogeneous fields.

Text S1: Optimum Setup Design

An optimum setup design could represent the Gravity Driven Convection (GDC) with smallest number of grids and shortest simulation time. To get a good setup design we need to know both the behavior of the GDC and the properties of the field and the fluid.

First, two basic features of GDC are used as references in designing the simulation setup. We use characteristic wave length (or earliest finger width) ℓ_c to assist designing the grid and domain sizes, and use the characteristic onset time τ_c to assist setting the simulation time. They are, respectively, given as

$$\ell_c = \ell_c^* \frac{\mu\phi D}{\Delta\rho g \kappa_g} \tag{1}$$

and

$$\tau_c = \tau_c^* \frac{(\mu\phi)^2 D}{(\Delta\rho g \kappa_g)^2}, \tag{2}$$

where, ℓ_c^* and τ_c^* are, respectively, dimensionless characteristic wavelength and onset time, which are constants obtained from theoretical, numerical or experimental studies; μ is the viscosity; ϕ is the porosity; D is the diffusion coefficient; $\Delta\rho$ is the maximum density increase due to CO_2 dissolution; g is the gravitational acceleration; κ_g is the geometric mean permeability. For homogeneous media, the empirical values for ℓ_c^* and τ_c^* are listed in Table S1, which also contains the results from this study.

The domain size should be large enough to cover enough number of convection fingers, while the grid size should be smaller than or close to the size of convection fingers. From our testing simulations (see Figures S1 and S2), we find that the domain size of $30L_c \times 30L_c$ and grid size of $0.3L_c \times 0.3L_c$ are enough to describe the GDC. Increasing the domain size to $60L_c \times 30L_c$ and $30L_c \times 60L_c$ or reducing the grid size to $0.15L_c \times 0.3L_c$, $0.3L_c \times 0.15L_c$

and $0.15L_c \times 0.075L_c$ does not systematically affect the onset time and dissolution rate. We notice that reducing or increasing the (especially vertical) grid size could significantly affect the characteristic wave length (i.e., the width of earliest unstable fingers) but this does not affect the statistic dissolution rate. Results from Elenius et al. (2015) show that the dissolution can be correctly simulated even if the grid size is several times larger than the characteristic wave length, although the concentration profile is not precisely represented. For homogeneous fields, a simulation time of $6\tau_c$ is enough to obtain the asymptotic dissolution rate. For heterogeneous fields, the simulation is not terminated until the fast unstable finger touches the bottom, to make sure the finger has ergodically traveled the heterogeneous domain; here, we define the finger has touched the bottom when the maximum CO_2(aq) concentration on the bottom increases to 25% of the maximum CO_2(aq) concentration.

Second, for numerical simulations in heterogeneous fields, we need also to take into account the correlation length scale. The domain size should be, if possible, 4 times larger than the correlation length scale which should be at least 5 times larger than the grid size. Because the domain size is $30L_c$, the correlation length should be less than $10L_c$. Because the grid size is $0.3L_c$, the minimum correlation length is $1.5L_c$. Here, maximum employed correlation length is $8L_c$ and minimum employed correlation length is $2L_c$. Additionally, the horizontally layered formation is used to represent the infinite correlation length in the horizontal direction.

Text S2: Gravity-Driven Convection in Reference Homogeneous Fields

We begin the analysis of Gravity-Driven Convection (GDC) from the results in homogeneous fields. The analysis of GDC in homogeneous field is given for two reasons. First, the analysis on GDC in homogeneous field serves as benchmark of the numerical algorithm, since it has been well studied in literature. Second, it shares the general behavior of GDC, and thus it serves as reference for the heterogeneous field.

From Figure S3, we can see that the dimensionless dissolution rate in homogeneous media (F^*) initially follows the pure diffusion function, until when $t^* \approx 500$, after that, the dissolution rate increases due to the gravity driven convection enhances the dissolution rate. The dissolution rate finally reaches the asymptotic value of around 0.09. This dissolution rate ($F^* \approx$0.09) obtained in this work is slightly larger than 0.075 in Elenius & Johannsen (2012) and 0.065 in Martinez & Hesse (2016); in the latter the Capillary Transition Zone (CTZ) boundary is employed. If we compare the dissolution rate to the vertical and horizontal finger velocities, we can see that the increase of dissolution rate is accompanied by the increase of the vertical and horizontal finger velocities. This implies that the dissolution rate is dominated by advection when gravity-driven instability appears. The vertical finger velocity is around 0.30, which is larger than 0.21 obtained in Elenius & Johannsen (2012), because impermeable top boundary is employed in the latter study.

Here, we specially note that the onset time for the enhanced dissolution is defined as nonlinear onset time, which is the time when instability fingers emerge (Elenius & Johannsen, 2012). If we observe the middle panel of Figure S3, we can find that the vertical finger velocity first decreases and then increases at around $t^* = 250$. Hidalgo & Carrera

(2009) also show the flow rate initially decreases and then increases to a constant value. The time at the inflection point is defined as linear onset time (Elenius & Johannsen, 2012). Here, we only consider the nonlinear onset time because it is more related to the dissolution efficiency in practice. The nonlinear onset time is affected by the initial perturbation, the field heterogeneity and the computational accuracy. For the real heterogeneous field, the nonlinear onset time is negligibly small, as shown in the paper supported by this document.

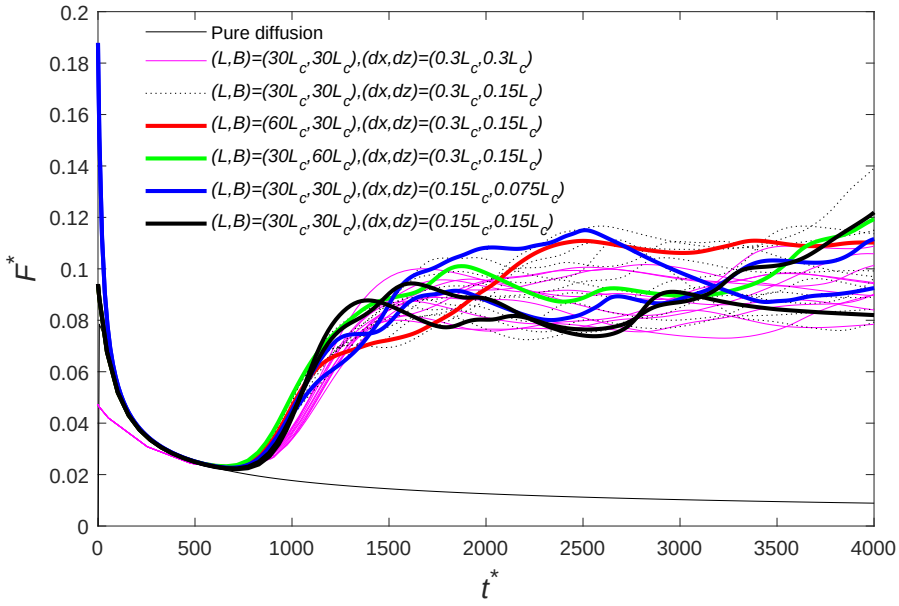

Figure S1: Analysis of the effect of grid size on the the dissolution rate.

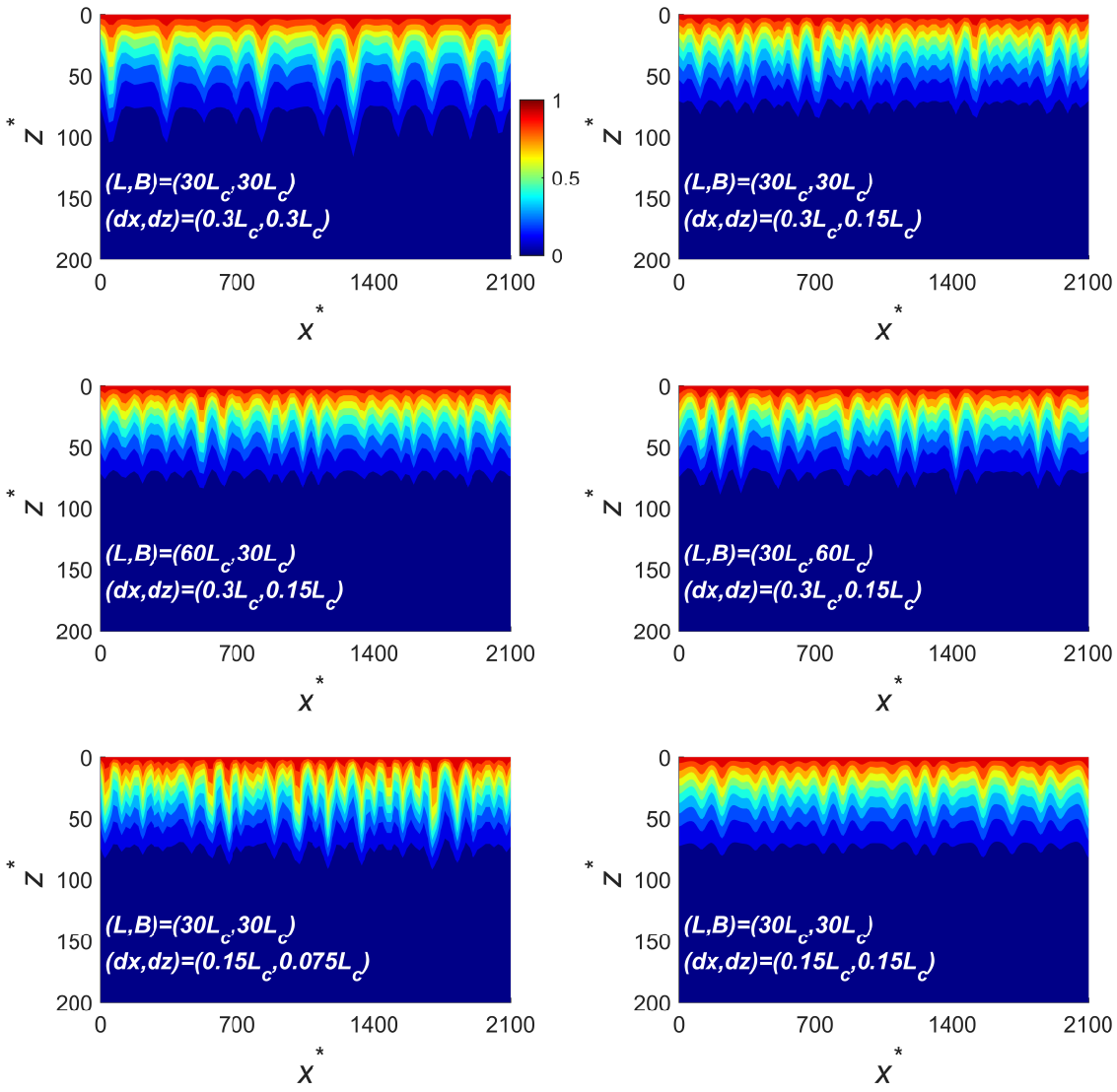

Figure S2: Analysis of the effect of grid size on the finger size(for the case of $(L, B) = (60L_c, 30L_c)$, $(dx, dz) = (0.3L_c, 0.15L_c)$, we only show $x \in (0, 30L_c)$).

Table S1: Published data for dimensionless onset time (τ_c^*) and dimensionless wave length (ℓ_c^*) for (isotropic) homogeneous field.

Onset time (τ_c^*)	**Wave length** (ℓ_c^*)	**Top boundary**	**Method**	**Reference**
30,75	95	-	Theor.	Ennis-King et al. (2005)
78	92	-	Theor.	Ennis-King & Paterson (2005)
75	96	-	Theor.	Xu et al. (2006)
1,156- 1,412	34-38	diff. only[a]	Num.	Pruess & Zhang (2008)
146	90	-	Theor.	Riaz et al. (2006)
1,000- 5,000	-	diff. only	Num.	Pau et al. (2010)
47.9	115.3	-	Theor.	Cheng et al. (2012)
3,500	-	diff. only	Num..	Cheng et al. (2012)
4,860	170	diff. only	Num.	Elenius & Johannsen (2012)
31	73	-	Theor.	Elenius et al. (2012)
5800	-	diff. only	Num.	Elenius et al. (2012)
2500	-	CTZ[b]	Num.	Elenius et al. (2012)
845	-	diff. only	Num.	Azin et al. (2013)
1,200	80-140	diff. only	Num.	Slim (2014)
56	-	-	Theor.	Jafari Raad et al. (2016)
$Ra^{0.8573}$	-	Permeable	Exp.	Rasmusson et al. (2017)
500	70	Permeable	Num.	This study

[a] The top boundary only allows mass to go through the boundary via diffusion.

[b] The top boundary is capillary transition zone.

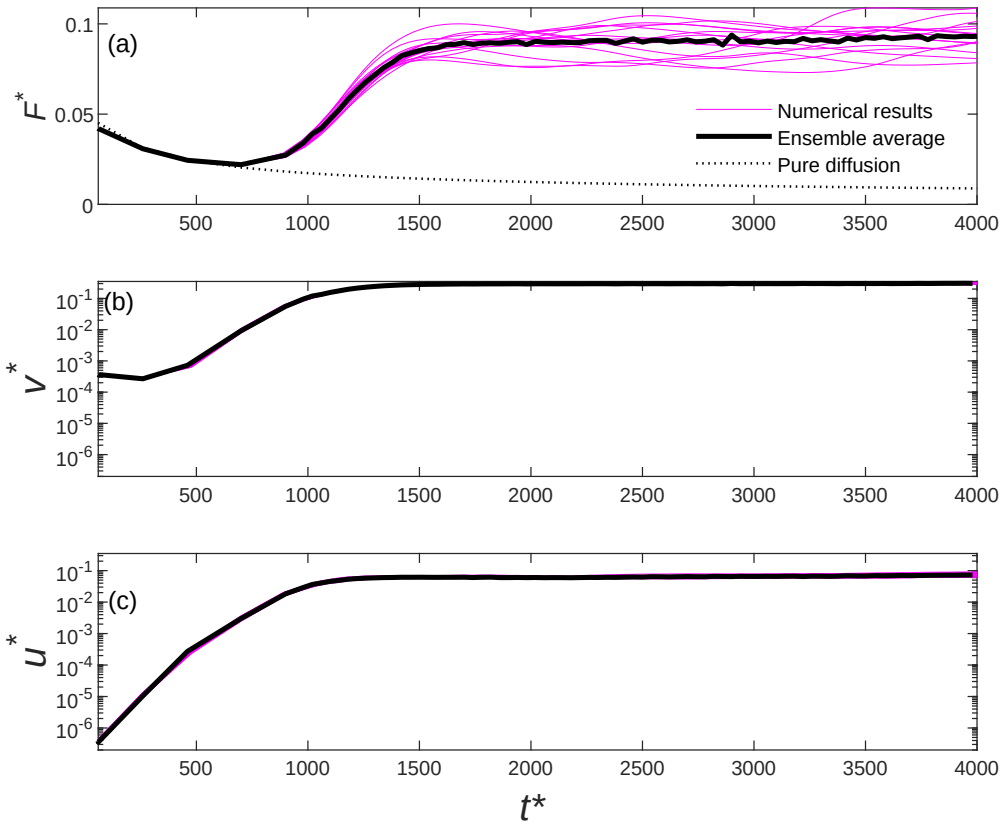

Figure S3: Homogeneous case: temporal developments of dimensionless dissolution rate (top), dimensionless vertical finger velocity (middle) and dimensionless horizontal finger velocity (bottom).

References

Azin, R., Raad, S. M. J., Osfouri, S., & Fatehi, R. (2013). Onset of instability in CO2 sequestration into saline aquifer: Scaling relationship and the effect of perturbed boundary. *Heat and Mass Transfer*. doi: 10.1007/s00231-013-1199-7

Cheng, P., Bestehorn, M., & Firoozabadi, A. (2012). Effect of permeability anisotropy on buoyancy-driven flow for CO 2 sequestration in saline aquifers. *Water Resources Research*. doi: 10.1029/2012WR011939

Elenius, M. T., & Johannsen, K. (2012). On the time scales of nonlinear instability in miscible displacement porous media flow. *Computational Geosciences*, *16*(4), 901-911. Retrieved from `https://doi.org/10.1007/s10596-012-9294-2` doi: 10.1007/s10596-012-9294-2

Elenius, M. T., Nordbotten, J. M., & Kalisch, H. (2012). Effects of a capillary transition zone on the stability of a diffusive boundary layer. *IMA Journal of Applied Mathematics (Institute of Mathematics and Its Applications)*. doi: 10.1093/imamat/hxs054

Elenius, M. T., Voskov, D. V., & Tchelepi, H. A. (2015). Interactions between gravity currents and convective dissolution. *Advances in Water Resources*. doi: 10.1016/j.advwatres.2015.05.006

Ennis-King, J., & Paterson, L. (2005). Role of convective mixing in the long-term storage of carbon dioxide in deep saline formations. *SPE Journal*. doi: 10.2118/84344-PA

Ennis-King, J., Preston, I., & Paterson, L. (2005). Onset of convection in anisotropic porous media subject to a rapid change in boundary conditions. *Physics of Fluids*. doi: 10.1063/1.2033911

Hidalgo, J. J., & Carrera, J. (2009). Effect of dispersion on the onset of convection during co2 sequestration. *Journal of Fluid Mechanics*, *640*, 441–452.

Jafari Raad, S. M., Emami-Meybodi, H., & Hassanzadeh, H. (2016). On the choice of analogue fluids in co2 convective dissolution experiments. *Water Resources Research*, *52*(6), 4458-4468. Retrieved from https://agupubs.onlinelibrary.wiley.com/doi/abs/10.1002/2015WR018040 doi: 10.1002/2015WR018040

Martinez, M. J., & Hesse, M. A. (2016). Two-phase convective co2 dissolution in saline aquifers. *Water Resources Research*, *52*(1), 585-599. Retrieved from https://agupubs.onlinelibrary.wiley.com/doi/abs/10.1002/2015WR017085 doi: 10.1002/2015WR017085

Pau, G. S., Bell, J. B., Pruess, K., Almgren, A. S., Lijewski, M. J., & Zhang, K. (2010). High-resolution simulation and characterization of density-driven flow in co2 storage in saline aquifers. *Advances in Water Resources*, *33*(4), 443 - 455. Retrieved from http://www.sciencedirect.com/science/article/pii/S0309170810000217 doi: https://doi.org/10.1016/j.advwatres.2010.01.009

Pruess, K., & Zhang, K. (2008). Numerical Modeling Studies of The Dissolution-Diffusion-Convection Process During CO2 Storage in Saline Aquifers. *Lawrence Berkeley National Laboratory*.

Rasmusson, M., Fagerlund, F., Rasmusson, K., Tsang, Y., & Niemi, A. (2017). Refractive-Light-Transmission Technique Applied to Density-Driven Convective Mixing in Porous Media With Implications for Geological CO2 Storage. *Water Resources Research*. doi: 10.1002/2017WR020730

Riaz, A., HESSE, M., TCHELEPI, H. A., & ORR, F. M. (2006). Onset of convection in a gravitationally unstable diffusive boundary layer in porous media. *Journal of Fluid Mechanics*, *548*, 87–111. doi: 10.1017/S0022112005007494

Slim, A. C. (2014). Solutal-convection regimes in a two-dimensional porous medium. *Journal*

of Fluid Mechanics, *741*, 461–491. doi: 10.1017/jfm.2013.673

Xu, X., Chen, S., & Zhang, D. (2006). Convective stability analysis of the long-term storage of carbon dioxide in deep saline aquifers. *Advances in Water Resources*. doi: 10.1007/s11432-006-0397-z